Original Article

MOLECULAR METABOLISM

Physiological roles of the GIP receptor in murine brown adipose tissue

Jacqueline L. Beaudry [1], Kiran D. Kaur [1], Elodie M. Varin [1], Laurie L. Baggio [1], Xiemin Cao [1], Erin E. Mulvihill [1,3], Holly E. Bates [1,4], Jonathan E. Campbell [1,5], Daniel J. Drucker [1,2,*]

ABSTRACT

Objective: Glucose-dependent insulinotropic polypeptide (GIP) is secreted from the gut in response to nutrient ingestion and promotes meal-dependent insulin secretion and lipid metabolism. Loss or attenuation of GIP receptor (GIPR) action leads to resistance to diet-induced obesity through incompletely understood mechanisms. The GIPR is expressed in white adipose tissue; however, its putative role in brown adipose tissue (BAT) has not been explored.

Methods: We investigated the role of the GIPR in BAT cells *in vitro* and in BAT-specific ($Gipr^{BAT-/-}$) knockout mice with selective elimination of the *Gipr* within the $Myf5^{+}$ expression domain. We analyzed body weight, adiposity, glucose homeostasis, insulin and lipid tolerance, energy expenditure, food intake, body temperature, and iBAT oxygen consumption *ex vivo*. High-fat diet (HFD)-fed $Gipr^{BAT-/-}$ mice were studied at room temperature (21 °C), 4 °C, and 30 °C ambient temperatures.

Results: The mouse *Gipr* gene is expressed in BAT, and GIP directly increased *Il6* mRNA and IL-6 secretion in BAT cells. Additionally, levels of thermogenic, lipid and inflammation mRNA transcripts were altered in BAT cells transfected with *Gipr* siRNA. Body weight gain, energy expenditure, and glucose and insulin tolerance were normal in HFD-fed $Gipr^{BAT-/-}$ mice housed at room temperature. However, $Gipr^{BAT-/-}$ mice exhibited higher body temperatures during an acute cold challenge and a lower respiratory exchange ratio and impaired lipid tolerance at 21 °C. In contrast, body weight was lower and iBAT oxygen consumption was higher in HFD-fed mice housed at 4 °C but not at 30 °C.

Conclusions: The BAT GIPR is linked to the control of metabolic gene expression, fuel utilization, and oxygen consumption. However, the selective loss of the GIPR within BAT is insufficient to recapitulate the findings of decreased weight gain and resistance to obesity arising in experimental models with systemic disruption of GIP action.

Keywords Glucose-dependent insulinotropic polypeptide receptor; Brown adipose tissue; Thermogenesis; Energy expenditure; Obesity; Lipid metabolism

1. INTRODUCTION

The gastrointestinal tract plays a dominant role in the digestion and assimilation of nutrients, enabling integrated control of energy homeostasis [1]. Two gut-derived hormones, glucagon-like peptide-1 (GLP-1) and glucose-dependent insulinotropic polypeptide (GIP) potentiate glucose-dependent insulin secretion via cognate receptors on islet β-cells [2]. Notably, both peptides also exert a wide range of extra-pancreatic activities. GLP-1 controls appetite, attenuates gut motility, decreases chylomicron secretion, promotes natriuresis, and attenuates inflammation, actions mediated through the GLP-1 receptor (GLP-1R) [3]. Indeed, these actions are conserved in human subjects, supporting the development of GLP-1R agonists for the treatment of type 2 diabetes and obesity.

The extrapancreatic actions of GIP have been less extensively characterized but include promotion of lipid uptake in adipose tissue, stimulation of bone formation, and regulation of cardiac lipid metabolism [2,4]. Potentiation of the insulinotropic action of GIP contributes to the glucoregulation ensuing following inhibition of dipeptidyl peptidase-4, a ubiquitous enzyme regulating the cleavage and inactivation of GIP and GLP-1 [5,6]. In contrast to GLP-1, molecules based on GIP action are not currently utilized as therapeutic agents for the control of metabolic disorders. Indeed, the glucoregulatory actions of GIP are impaired in the context of diabetes, although improvement of glycemia following insulin administration over 4 weeks enabled the partial restoration of GIP action in subjects with type 2 diabetes [7]. Paradoxically, loss of GIP action is also associated with improvement in experimental diabetes and resistance to diet-induced obesity [2,4].

[1]Lunenfeld-Tanenbaum Research Institute, Mt. Sinai Hospital, Toronto, Ontario, Canada [2]Department of Medicine, University of Toronto, Toronto, Ontario, Canada

[3] Current address: University of Ottawa Heart Institute, 40 Ruskin Street, Ottawa, ON H-3228A, KIY 4W7, Canada.
[4] Current address: Trent University, Biology, 2140 East Bank Drive, Peterborough, ON, K9L 1Z8, Canada.
[5] Current address: Duke Molecular Physiology Institute, 49—102, 300 N. Duke St. Durham, NC 27701, USA.

*Corresponding author. Lunenfeld-Tanenbaum Research Institute, Mt. Sinai Hospital, 600 University Avenue TCP5-1004, Toronto, ON, M5G 1X5, Canada. E-mail: drucker@lunenfeld.ca (D.J. Drucker).

Received June 28, 2019 • Revision received July 27, 2019 • Accepted August 6, 2019 • Available online 10 August 2019

https://doi.org/10.1016/j.molmet.2019.08.006

Indeed, these findings have been achieved with a broad number of experimental approaches, including genetic inactivation of the GIP receptor (*Gipr*) [8], disruption of the *Gip* gene in mice [9], as well as GIPR blockade using receptor antagonists, or immunoneutralization of the GIP peptide in mice, rats, and non-human primates [10,11]. Moreover, genetic variation in the human *GIPR* gene associates with body mass index and visceral fat accumulation in several different populations [12–14]. Nevertheless, it remains unclear how central or peripheral loss of GIP action engages circuits leading to the reduction of food intake, modulation of fat storage, or control of energy expenditure.

Several studies have implicated GIP action within white adipose tissue in the control of energy storage and body weight, however, the actions of GIP in adipose tissue remain incompletely understood, and at times, controversial [2,4]. Whole body germline inactivation of the *Gipr* gene in mice leads to resistance to diet-induced obesity, associated with preservation of whole body oxygen consumption despite prolonged high-fat diet feeding [8]. Reduction of GIP secretion in high-fat diet fed mice also leads to reduced body weight gain and decreased adipose tissue mass, accompanied by increases in energy expenditure [9]. Consistent with these findings, we demonstrated increased energy expenditure throughout the light and dark cycles in $Gipr^{-/-}$ mice maintained on both regular chow and high-fat diets, associated with increased levels of uncoupling protein–1 (UCP-1) mRNA transcripts in BAT [15]. Nevertheless, the functional importance of the BAT GIPR has not been defined. Here, we assessed the metabolic importance of the GIPR in BAT cells and in newly generated mice with selective inactivation of the GIPR in BAT.

2. METHODS AND MATERIALS

2.1. Animal models

All animal experiments were conducted in accordance with protocols approved by the Toronto Centre for Phenogenomics (TCP) Animal Care Committee (AUP# 20-0045H). The generation and characterization of $Gipr^{-/-}$ and floxed mice has been described previously [16,17]. Male and female $Gipr^{BAT-/-}$ (BAT-specific *Gipr* knockout) mice and littermate controls, $Gipr^{BAT+/+}$ were generated by crossing hemizygous *Myf5*-Cre mice (007893, The Jackson Laboratory, Bar Harbor, ME) with $Gipr^{Flox/Flox}$ mice that were maintained on a C57BL/6J background. *Myf5*-Cre, $Gipr^{Flox/Flox}$, and Wild-Type (WT) mice were pooled as a single $Gipr^{BAT+/+}$ control group, as these mice were phenotypically similar in terms of body weight, fat and lean mass, and glucose homeostasis. Littermate male mice were group-housed and maintained on a 12h light/dark cycle at room temperature (RT; 21 °C) with free access to food and water, except where indicated. Mice were fed a standard rodent chow diet (RCD; 18% kcal from fat, 2018 Harlan Teklad, Mississauga, ON) or high-fat diet (HFD; 45% kcal from fat, D12451i, Research Diets, New Brunswick, NJ) for diet-induced obesity analyses for 32 weeks (starting at 8–10 weeks of age until ~ 40 weeks of age), as indicated in the figure legends.

In a separate experiment, male $Gipr^{BAT+/+}$ and $Gipr^{BAT-/-}$ mice were housed as described above at 4 °C for approximately 12 weeks in non-vented microisolator cages (Ancare, Bellmore, NY) held in environmentally controlled enclosures (Betatech Inc., Barrie, ON) with free access to HFD food and water. Starting at 8–10 weeks of age, mice were gradually acclimated to cold temperatures by first transferring them to 16 °C and subsequently, decreasing the temperature by 2 °C every day until 4 °C was reached.

All mice were euthanized by CO_2 inhalation, and tissues were immediately frozen in liquid nitrogen. Adipose tissues are abbreviated as follows: inguinal white adipose tissue (iWAT), epididymal white adipose tissue (eWAT), retroperitoneal white adipose tissue (rWAT), mesenteric white adipose tissue (mWAT), interscapular brown adipose tissue (iBAT).

2.2. Cell line studies

Immortalized BAT cells were obtained from Dr. Bruce Spiegelman's laboratory (Department of Cancer Biology, Dana-Farber Cancer Institute, Boston, MA) [18]. BAT pre-adipocyte cells were cultured on collagen-coated 12-well plates at a seeding density of 40,000 per well at 37 °C, CO_2 0.5%, in growth media (DMEM (4.5 g/l glucose, L-glutamine, Wisent, St. Bruno, QC) supplemented with 20% FBS (Wisent)), 1% Sodium Pyruvate (100 mM, Sigma), <0.01% HEPES (1M, Wisent), and 1% Penicillin-Streptomycin (Wisent). Once a healthy mono-layer was achieved, growth media was replaced with induction media (DMEM supplemented with 10% FBS, 1% Sodium Pyruvate, <0.01% HEPES, 1% Penicillin-Streptomycin, 2 mg/ml dexamethasone (Sigma), 0.5 mM 3-isobutyl-1-methylxanthine (IBMX; Sigma), 125 mM indomethacin (Sigma), 10 mg/ml or 1.7 mM insulin (Sigma), and 1 nM T3 (Triiodo-L-Thyronine, Sigma)). After a 48 hr induction period, media was switched to maintenance media (DMEM supplemented with 10% FBS, 1% Sodium Pyruvate, <0.01% HEPES, 1% Penicillin-Streptomycin, 10 mg/ml or 1.7 mM insulin and 1 nM T3) and replaced as required until cells were fully differentiated by Day 7. All experiments were performed on fully differentiated cells on Day 7.

To assess the effects of acute [D-Ala^2]-GIP (Chi Scientific, Maynard, MA) on gene expression, BAT cells were differentiated for 7 days in 12-well plates as described above. On Day 7, BAT cells were cultured in nutrient-starved media for 3 hr in FBS-free DMEM media devoid of all supplements except sodium pyruvate and HEPES. After 3 hr of starvation, BAT cells were treated with media (1 ml) containing either PBS or [D-Ala^2]-GIP (100 nM) for times as indicated. Total RNA was isolated by adding 1 ml of Tri Reagent to each well and homogenizing cells by repetitive pipetting.

For cell transfection, on day 4 of differentiation, BAT cells were trypsinized (Wisent, QC) and re-plated with transfection complexes suspended in antibiotic-free maintenance media in sterile collagen-coated 12-well plates containing 800,000–1,000,000 cells per well. Transfection complexes consisted of siRNA duplexes (Universal scrambled negative control (Origene, Rockville, MD) sequence, Cat# SR30004-CGUUAAUCGCGUAUAAUACGCGUAT) or *Gipr* (Origene duplex sequence, Cat# SR406328C-CGCACUCCCAUCCUAAUAACCAUCT) diluted in OptiMEM to a final concentration of 80 nM in 1 ml of media, using Lipofectamine RNAiMAX Reagent (Thermo Fisher Scientific), following the manufacturer's protocol. Maintenance media was replaced as required until Day 7 when cells were harvested for RNA isolation as described above.

For Seahorse studies, BAT cells were differentiated until Day 6 and then trypsinized and re-plated into a collagen-coated Seahorse XF96 cell culture plate (Agilent, Mississauga, ON) at a seeding density of 15,000 cells per well in maintenance media. On Day 7, healthy cells were serum-starved for 2 h in DMEM media without sodium bicarbonate (Cat#, 219-010-LK, Wisent, QC). Oxygen consumption rate (OCR) of BAT cells was determined using an XF96 Extracellular Flux Analyzer (Seahorse Bioscience, Agilent). Uncoupled and maximal OCR were determined using oligomycin (1.5 μM, Sigma) and FCCP (1 μM, Sigma). Antimycin A and rotenone (1 μM, Sigma) were used to inhibit Complex III- and Complex I- dependent respiration. All measurements

were normalized to cell number per well by DNA quantification using a CyQuant kit (Cat# C35006, Invitrogen Canada, Burlington, ON).

2.3. Food intake and body composition

Food intake was measured at 30–32 weeks of HFD feeding. Mice were housed individually in cages containing pre-weighed amounts of food. After 72 hr, food was re-weighed, and food intake was averaged per gram body weight per day for each mouse. Body weight was measured every 2 weeks for all mice. Body composition was measured in the morning, prior to HFD initiation, and after 32 weeks on HFD using an EchoMRI nuclear magnetic resonance system (EchoMRI LLC, Houston, TX).

2.4. Body temperature

Body temperature was measured using a rectal thermometer (Thermoworks) coated in Vaseline® after a ~16 hr fast. Body temperature data are from mice prior to commencement of HFD and after 10–12 and 30–32 weeks of HFD diet, as indicated. For body temperature experiments during an acute cold challenge performed in *Gipr*$^{-/-}$ mice, experiments were performed in mice fasted for ~16 hr while being housed at room temperature or 30 °C. Body temperature was measured every hour for 6 hr while animals were housed at 4 °C with no access to food in clear pre-cooled plastic cages.

2.5. Energy expenditure

To measure basal energy expenditure, animals were placed into metabolic chambers after 16–18 weeks on HFD for a 72 hr period. After an overnight acclimation period, measurements of oxygen consumption, carbon dioxide production, respiratory exchange ratio (RER), activity, and energy expenditure (kcal/hr) were recorded using the Comprehensive Lab Animal Monitoring System (CLAMS; Columbus Instruments, Columbus OH). Data were averaged every hour and are expressed as heat or energy expenditure (kcal/hr).

To measure non-shivering thermogenesis, acute injections of CL316,243 (Sigma), a selective β-3-adrenergic receptor agonist, were administered to mice that were anesthetized with sodium pentobarbital (60 mg/kg). Mice were placed on a heating pad for 10 mins prior to transferring them into a CLAMS chamber on a heating pad where they were acclimatized for ~8 mins and were subsequently given ip injections of vehicle control (PBS) or CL316,243 (1 mg/kg). Measurements were recorded every 15 s, and the response to CL316,243 was measured by a percentage change from the average baseline (oxygen consumption after PBS injection) of each individual mouse. Data are presented as the area under the curve during the PBS and the response to CL316,243.

To measure more chronic thermogenic responses, mice were injected with CL316,243 (1 mg/kg) for 1–3 days. Mice were placed into metabolic chambers with fresh food and water for a total of 4 days. They received an ip injection of PBS at ~ 9–10 AM and ~ 4–5 PM on the first day and then twice-daily ip injections of CL316,243 (1 mg/kg) for 1–3 days at similar times to PBS administration. Data from these measurements are represented as described above. Data were averaged every hour and expressed as heat and energy expenditure (kcal/hr). Mice that were housed at 4 °C were only given CL316,243 treatments for 24 h as all metabolic experiments were recorded at room temperature.

2.6. Glucose, insulin, and lipid tolerance tests

For glucose tolerance tests, D-Glucose (1.5 g/kg; Sigma, Oakville, ON) was administered by oral gavage (oGTT) or ip injection (ipGTT), as indicated. For insulin tolerance tests (ITT), animals received a single ip injection of 1.0 U/kg body weight of a rapid-acting insulin analogue (Humalog, VL7510, Eli Lily, Scarborough, ON). Due to increased insulin sensitivity, mice that were housed at 4 °C, received a single ip injection of 0.35 U/kg body weight of insulin. Blood glucose levels were measured from tail vein samples using a hand-held glucose monitor (Contour, Bayer, Mississauga, ON) as indicated post-glucose gavage or insulin injection. Samples were kept on ice, and plasma was collected in lithium/heparin coated tubes by centrifugation (>12, 000 rpm at 4 °C for 5 min) and stored at −80 °C until further analysis for hormone levels.

For lipid tolerance tests (LTT), animals received a 200 μl oral gavage of olive oil (Sigma) at time 0 and blood samples were collected before (time 0) and 1, 2, and 3 hrs after gavage. The above metabolic tests were performed 2 weeks apart in mice fed a HFD after 2–8 weeks, 22–28 weeks, or in mice housed at 4 °C for 2–8 weeks, as indicated. Only data from mice analyzed during 22-28 weeks of HFD feeding are shown for the glucose, insulin and lipid tolerance tests. All mice were fasted ~5 hrs prior to the beginning of each metabolic test.

2.7. Acute GIP injections

WT mice were fasted for ~4 hr and were administered 24 nmol/kg [D-Ala^2]-GIP (Chi Scientific, Maynard, MA) or PBS (vehicle). Blood was collected via tail vein and mixed with 10% volume of TED (5000 kIU/ml Trasylol (Bayer), 32 mM EDTA, and 0.01 mM Diprotin A (Sigma)) at 0, 30 min, 1 hr, and 2 hr.

2.8. Hormone analysis

IL-6 levels (Meso Scale Diagnostics, Cat# L45QXA-1, small spot assay system) were assessed in BAT cell media or plasma samples after acute GIP administration at the indicated times.

2.9. Non-esterified fatty acid and triglyceride analysis

Plasma non-esterified fatty acids (NEFAs) were measured using the NEFA-HR (2) kit (Wako Diagnostics, Cat# 999–34691, 995–34791, 991–34891, 993–35191, 276–76491, Mountain View, CA) or triglycerides (TGs) using the Trig-GB kit (Cat# 05171407, calibrator 11877771216, Roche, Mississauga, ON) were assessed in plasma samples after ~ 16 hr overnight fast and 1 hr refeed or during the LTT as described above.

For determination of TGs in tissue, frozen iBAT samples were weighed (10–20 mg) and TGs were extracted using a 2:1 chloroform-methanol solution, dried under N_2 and reconstituted in 50 μl of 3:2 tert-butyl alcohol:triton X-100/methyl alcohol (1:1) and quantified with a commercially available enzymatic assay kit (Trig-GB, Roche).

2.10. RNA isolation, cDNA, and qPCR

Tissue samples were dissected, weighed, frozen in liquid-nitrogen, and stored at −80 °C. Frozen tissues were homogenized in Tri Reagent (Molecular Research Center, Cincinnati, ON) using a TissueLyser II system (Qiagen, Germantown, MD), and total RNA was extracted using the manufacturer's protocol. First strand cDNA was synthesized from DNase I-treated total RNA (1–2 μg) using SuperScript III and random hexamers (Thermo Fisher Scientific, Markham, ON). Gene expression was quantified using a QuantStudio System and TaqMan Gene Expression Master Mix and Assays (Thermo Fisher Scientific). Primer/probes were purchased from Thermo Fisher Scientific and are listed in Supplementary Table 1. Gene expression data were analyzed by $2^{-\Delta\Delta Ct}$ method, and expression levels for each gene were normalized to *Actb* (β-actin) or *Tbp* (TATA-box-binding protein).

2.11. Full-length mouse *Gipr* PCR

Full-length (~1.4 kb) mouse *Gipr* transcripts were amplified from cDNA using the following primers: forward 5′-CTG CTT CTG CTG CTG TGGT -3′ and reverse 5′-CAC ATG CAG CAT CCC AGA-3′, separated on an agarose gel, transferred to a nylon membrane, and hybridized overnight with an internal ^{32}P-labeled mouse *Gipr*-specific oligonucleotide probe: 5′-CAT CCT TGG CAT CCT TGT TT-3'. Membranes were imaged using a Storm 860 Phosphor Screen and Quantity One imaging software (Bio-Rad, Hercules, CA). *Actb* or *Gapdh* was used as a control for RNA integrity of samples.

2.12. *Ex vivo* adipose tissue oxygen consumption

Oxygen consumption was assessed in fresh tissues from mice after CO_2 asphyxiation; tissues were immediately placed into warm (37 °C, DMEM (4.5 g/l glucose, L-glutamine, Wisent, St. Bruno, QC)) media. Tissues were weighed (~10–20 mg), washed in filtered warm 37 °C respiration buffer (PBS, 0.02% fatty acid free BSA, 25 μM glucose, 0.01% (vol/vol) of 100 mM Na pyruvate (Sigma)), minced with dissection scissors, re-suspended in 1 ml respiration buffer and placed into a Mitocell chamber (MT200A, Strathkelvin Instruments, North Lanarkshire, Scotland) with a Clark electrode (Strathkelvin). For each analyzed tissue, measurements were obtained from three pooled groups of fragments of equivalent size (~10–20 mg) and normalized to tissue weight.

2.13. Isolation of stromal vascular and mature adipocytes

Stromal vascular and enriched mature adipocyte fractions were isolated from iBAT pooled from 4 WT RCD mice at 12 weeks of age. iBAT was finely minced on ice, and then digested in a 50 ml conical vial for 30–50 min in a warm (37 °C) water bath, with gentle shaking in 1 mg/ml collagenase in HBSS supplemented with 3% BSA and 5 U/ml DNase I. Digestion was stopped once large pieces of adipose tissue could no longer be seen. Digested tissue was suspended in PBS supplemented with 10% FBS and the mixed solution was filtered through a 500 μm mesh. Stromal vascular and mature adipocyte fractions were separated and washed twice, by successive low speed centrifugations (1000–2000 rpm); the lipid-containing mature adipocytes floated to the top, and stromal vascular fraction pelleted at the bottom. Fractions were suspended in 1-2 ml of Trizol for RNA isolation and then stored at −80 °C until further analysis.

2.14. Statistical analysis

Statistical significance was determined between two groups using an unpaired two-tailed Student's t-test using GraphPad Prism version 8.0 software (San Diego, CA) and differences between more than two groups were examined by one-way ANOVA with a Tukey post-hoc test. A p value < 0.05 was considered statistically significant. An outlier test was performed using the GraphPad QuickCalcs Outlier Calculator. Data are represented as mean ± SEM, and the number of replicates per experiment can be found in the figure legends.

3. RESULTS

3.1. Whole body *Gipr*$^{-/-}$ mice maintain a higher body temperature in the cold and exhibit greater non-shivering thermogenic responses

Global loss of *Gipr* in mice is associated with resistance to diet-induced obesity [8,15,16,19], however the relative contributions of reduced food intake and/or increased energy expenditure to the phenotype of these animals remain unclear. We fed *Gipr*$^{-/-}$ mice a HFD for 30 weeks, housed them at 30 °C and performed an acute cold temperature challenge to determine how well these mice defended their body temperatures. *Gipr*$^{-/-}$ mice maintained a higher body temperature in the cold relative to WT littermate controls (Figure 1A). We next administered CL316,243 to determine non-shivering thermogenic responses after warm and cold acclimation. Regardless of acclimated ambient temperatures, *Gipr*$^{-/-}$ mice exhibited a greater non-shivering thermogenic response to CL316,243 administration (Figure 1B,C). Accordingly, these results prompted us to determine the importance of GIPR expression in BAT for whole body energy expenditure.

3.2. GIP directly regulates a thermogenic gene expression program in BAT cells

Gipr mRNA transcripts were detected in mouse adipose tissue depots including mWAT, iWAT, eWAT, rWAT, and iBAT (Figure 2A) at levels lower than detected in islets. The adipose tissue *Gipr* mRNA transcripts detected by qPCR corresponded to full-length *Gipr* mRNA (Figure 2B). Notably *Gipr* mRNA transcripts were simultaneously detected in the stromal vascular fraction (SVF), and to a greater extent in enriched mature adipocytes (Adipo) from fractionated iBAT (Figure 2B, Figure S1A). *Gipr* mRNA transcripts were also detected in a BAT cell line (Figure S1B) and increased during cell differentiation,

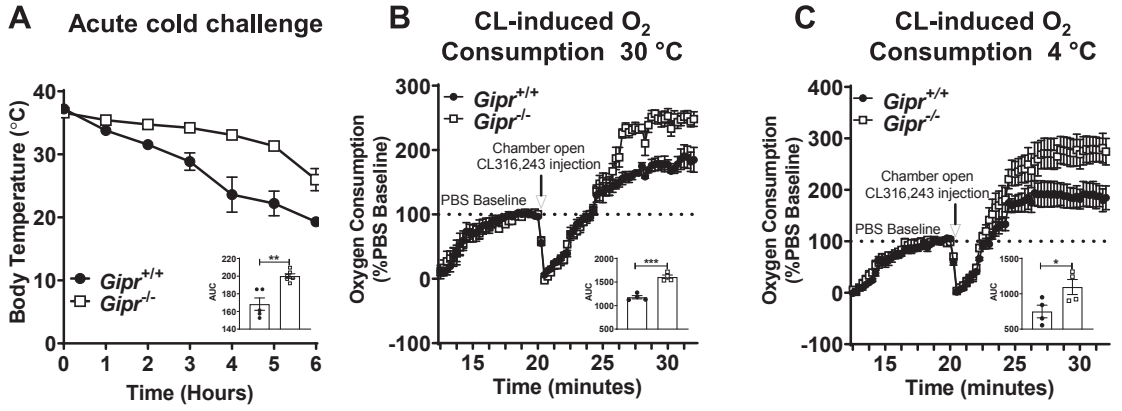

Figure 1: Global loss of *Gipr* increases body temperature regulation during acute cold challenge and non-shivering thermogenic responses in mice housed at cold or thermoneutrality. (A) Acute cold challenge in *Gipr*$^{-/-}$ mice, housed at 30 °C, fed a HFD for 30 weeks, n = 5–6. (B) CL316,243-induced O_2 consumption expressed relative to PBS response in *Gipr*$^{-/-}$ mice, housed at 30 °C, fed a HFD for 2 weeks, n = 4. (C) CL316,243-induced O_2 consumption expressed relative to PBS response in *Gipr*$^{-/-}$ mice, housed at 4 °C, fed a HFD for 2 weeks, n = 4. Data are represented as mean ± SEM. *p < 0.05, **p < 0.01, ***p < 0.001.

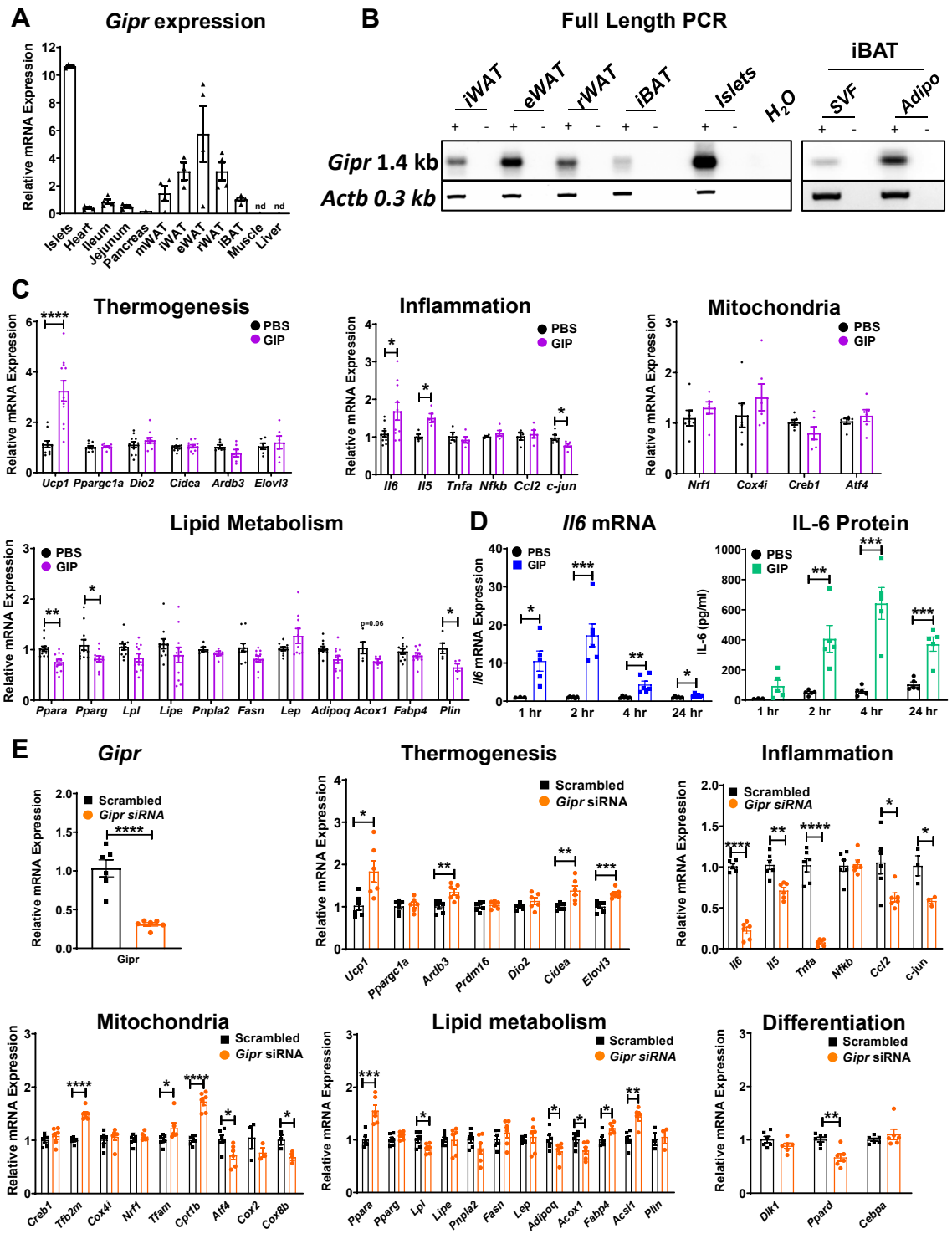

Figure 2: GIP increases IL-6 mRNA expression and protein levels while knockdown of *Gipr* modulates subsets of thermogenic, mitochondrial and inflammatory gene expression levels in BAT cells. (A) *Gipr* mRNA level was expressed relative to levels in pancreatic islets (determined using the standard curve method) in tissues from 20-week-old WT mice, fed a RCD, n = 4. (B) PCR and Southern blot analysis using a *Gipr*-specific internal oligonucleotide probe detected a full length (~1.4 kb) *Gipr* mRNA transcript in islets and adipose tissue, as well in stromal vascular (SVF) and enriched adipocyte (Adipo) fractions from pooled iBAT samples from WT mice fed a RCD. Analysis of *Actb* mRNA (~0.3 kb) within the same samples was used as a control. (C) mRNA transcript levels of thermogenic/inflammatory/mitochondrial/lipid metabolism genes in BAT cells (differentiated for 7 days) 4 hr after exposure to GIP (100 nM) expressed relative to levels in cells treated with PBS. (D) IL-6 mRNA and protein levels in BAT cells after 1, 2, 4, and 24 hr exposure to GIP (100 nM). (E) Basal levels of mRNA transcripts in differentiated BAT cells (7 days) transfected with scrambled control or *Gipr* siRNA. For C-E, levels of *Tbp* were used for normalization of relative mRNA expression levels. mWAT = mesenteric white adipose, iWAT = inguinal WAT, eWAT = epididymal WAT, rWAT = retroperitoneal WAT, iBAT = interscapular brown adipose tissue. Data are represented as mean ± SEM. *p < 0.05, **p < 0.01, ***p < 0.001, ****p < 0.0001. See also Figure S1.

coincident with induction of *Ppargc1a*, *Fabp4*, and *Adipoq* mRNA transcripts (Figure S1C). GIP treatment increased levels of *Ucp1*, *Il6*, and *Il5* and decreased levels of *c-Jun*, *Ppara*, *Pparg*, and *Plin* mRNA in BAT cells *in vitro* (Figure 2C). GIP also robustly increased *Il6* mRNA and secretion of IL-6 protein (Figure 2D), and plasma IL-6 levels were increased after acute GIP administration in WT mice (Figure S1D). Conversely, siRNA-mediated knockdown of *Gipr* in BAT cells increased levels of *Ucp1*, *Ardb3*, *Cidea*, *Elovl3*, *Tfb2m*, *Tfam*, *Cpt1b*, *Ppara*, *Fapb4*, and *Ascl*, and decreased levels of *Il6*, *Il5*, *Tnfa*, *Ccl2*, *c-Jun*, *Atf4*, *Cox8b, Lpl*, *Adipoq*, *Acox1*, and *Ppard* (Figure 2E). Basal oxygen consumption was similar but maximal oxygen consumption was higher in BAT cells with reduced levels of *Gipr* mRNA (Figure S1E). siRNA-mediated knockdown of *Gipr* in BAT cells was associated with differential gene expression responses to the adrenergic agonist CL316,243, with increased levels of *Ucp1*, *Cidea*, *Elovl3*, *Tfb2m*, *Cpt1b*, *Ppara*, *Fasn*, *Acsl1*,and *Nfkb* and decreased levels of *Atf4*, *Pparg*, *Lep*, *Il6*, *Tnfa*, and *Ccl2* (Figure S1F). Hence, both enhanced and reduced GIPR signaling regulates BAT genes linked to energy assimilation, BAT function, thermogenesis, and inflammation.

3.3. $Gipr^{BAT-/-}$ mice exhibit reduced basal RER and perturbed lipid tolerance

Loss of GIPR signaling attenuates weight gain following high-fat feeding [8,9,11,15]; yet, the mechanisms for this remain poorly understood. To determine whether the BAT GIPR contributes to basal control of energy homeostasis under HFD conditions, we crossed $Gipr^{flox/flox}$ with *Myf5*-Cre mice to generate $Gipr^{BAT-/-}$ mice (Figure S2A). Consistent with the expression domain of *Myf5*, levels of full length *Gipr* mRNA transcripts were markedly lower in iBAT and reduced in rWAT but not different in iWAT, eWAT, mWAT, pancreas, or heart from $Gipr^{BAT-/-}$ versus $Gipr^{BAT+/+}$ mice (Figure 3A, and Figure S2A). Lower levels of *Gipr* mRNA levels in rWAT is consistent with a substantial fraction of cells in this depot originating from the $Myf5^{+}$ cell lineage [20]. No differences in body weight (Figure 3B), fat and lean mass (Figure 3C), adipose tissue or organ weights (Figure S2B), food intake (Figure 3E), basal energy expenditure (Figure 3F), or activity levels (Figure S2C) were detected in HFD-fed $Gipr^{BAT-/-}$ mice housed at room temperature for 32 weeks. Fasted $Gipr^{BAT-/-}$ mice had higher body temperature at time 0 and maintained higher temperature during acute cold challenge (Figure 3D). $Gipr^{BAT-/-}$ mice transiently exhibited a lower basal RER, indicating increased lipid utilization (Figure 3G). We next examined energy expenditure after administration of CL316,243 for 3 days to determine if loss of *Gipr* in BAT influences BAT thermogenic responses. No differences in energy expenditure, RER, or activity levels were detected in mice injected twice daily with CL316,243 for 3 days (Figure 3H,I and Figure S2D), and oxygen consumption was not different in iBAT *ex vivo* (Figure 3J). $Gipr^{BAT-/-}$ mice displayed modestly higher lipid excursions during lipid challenge (Figure 3K), but no differences in iBAT TG content were detected (Figure 3L). Levels of mRNA transcripts for *Cidea*, *Ardb3*, and *Ppara* were lower and *Lipe* was higher in iBAT from $Gipr^{BAT-/-}$ mice (Figure 3M). Glucose and insulin tolerance, and plasma NEFAs were similar in $Gipr^{BAT+/+}$ vs. $Gipr^{BAT-/-}$ mice (Figure S2E—H). Plasma triglycerides were higher in the fasted and fed states in $Gipr^{BAT-/-}$ mice (Figure S2I); however, lipid tolerance was not different in $Gipr^{BAT-/-}$ mice on a HFD for 28 weeks (Figure S2J). Body temperatures were higher in $Gipr^{BAT-/-}$ mice fed a RCD after an overnight fast; however, no temperature differences were observed during an acute cold challenge (Figure S2K).

3.4. HFD-fed $Gipr^{BAT-/-}$ mice have higher fasted lipid levels however body weight and glucose homeostasis are normal when mice are housed at 30 °C

To explore the temperature-dependence of phenotypes in $Gipr^{BAT-/-}$ mice, we studied independent cohorts of mice at 30 °C after prolonged HFD feeding. No differences in body weight, fat and lean mass, body temperature, food intake (Figure 4A—D), basal or CL316,246-induced energy expenditure, RER, activity, tissues weights, iBAT O_2 consumption, lipid tolerance, or iBAT triglyceride content were detected (Figure 4E—K and Figure S3A-C) in $Gipr^{BAT-/-}$ mice studied at thermoneutrality after prolonged HFD feeding. Oral glucose tolerance was modestly impaired when mice were housed for 22 weeks and fed a HFD at thermoneutrality (Figure S3D), but no differences in ip glucose tolerance or insulin sensitivity (Figure S3E, S3F) were detected. In contrast, fasted plasma NEFAs and TGs were higher in $Gipr^{BAT-/-}$ mice housed at 30 °C (Figure 4L,M), suggesting that the impaired lipid homeostasis observed in $Gipr^{BAT-/-}$ mice at room temperature was independent of stimulated thermogenesis.

3.5. HFD-fed $Gipr^{BAT-/-}$ mice have lower body weight and iBAT mass when housed at 4 °C

To further evaluate the influence of ambient temperature on phenotypes exhibited by $Gipr^{BAT-/-}$ mice, we studied mice fed a HFD and chronically housed at 4 °C. $Gipr^{BAT-/-}$ mice exhibited lower body weight after 4—12 weeks (Figure 5A), fat and lean mass trended lower (Figure 5B), and iBAT mass was lower (Figure 4C). However, iWAT, eWAT, or rWAT mass and other organ weights were not different (Figure 5C, Figure S4A). Likewise, food intake (Figure 5D), basal energy expenditure (Figure 5E), RER (Figure 5F), activity (Figure S4B), or CL-induced energy expenditure (Figure 5G) or activity (Figure S4C) were also not different. $Gipr^{BAT-/-}$ mice had higher RER levels after administration of CL316,246 (Figure 5H). Basal O_2 consumption was higher in iBAT (Figure 5I), and iWAT (Figure 5J) in $Gipr^{BAT-/-}$ mice after 6 weeks at 4 °C, whereas O_2 consumption was not different in liver, eWAT and muscle, notwithstanding the small number of replicates analyzed (Figure 5K—M). Levels of mRNA transcripts for mitochondrial genes such as *Nrf1* and *Cox2* were modestly higher in iBAT from $Gipr^{BAT-/-}$ mice; yet, levels of the majority of mRNA transcripts examined were not different (Figure 5N). Glucose tolerance and insulin sensitivity (Figure S4D, E, G), fasted and refed plasma NEFAs (Figure S4H) and TGs (Figure S4I) were not different. $Gipr^{BAT-/-}$ mice had modestly lower TGs in response to an oral lipid challenge (Figure S4J); however, iBAT TG content was not different (Figure S4K).

4. DISCUSSION

Interest in the biological actions of GIP impinging on energy homeostasis has been bolstered by development of co-agonists with GIPR activity and by emerging data with GIPR antagonists. Notably, several GIPR co-agonists reduced fat mass, decreased body weight and improved glucose control in non-human primates [21] and in human subjects with type 2 diabetes [21,22]. Moreover, tirzepatide, an acylated GIPR-GLP-1R co-agonist, produced more weight loss than semaglutide and decreased fat mass, reduced food intake, and enhanced energy expenditure in mice with diet-induced obesity [23]. Impressively, tirzepatide administration reduced glycosylated hemoglobin and resulted in ~10 kg of weight loss in a 26-week Phase 2 clinical trial in human subjects with type 2 diabetes [24]. Although GIPR agonism enhances the metabolic effects of co-administered GLP-1R

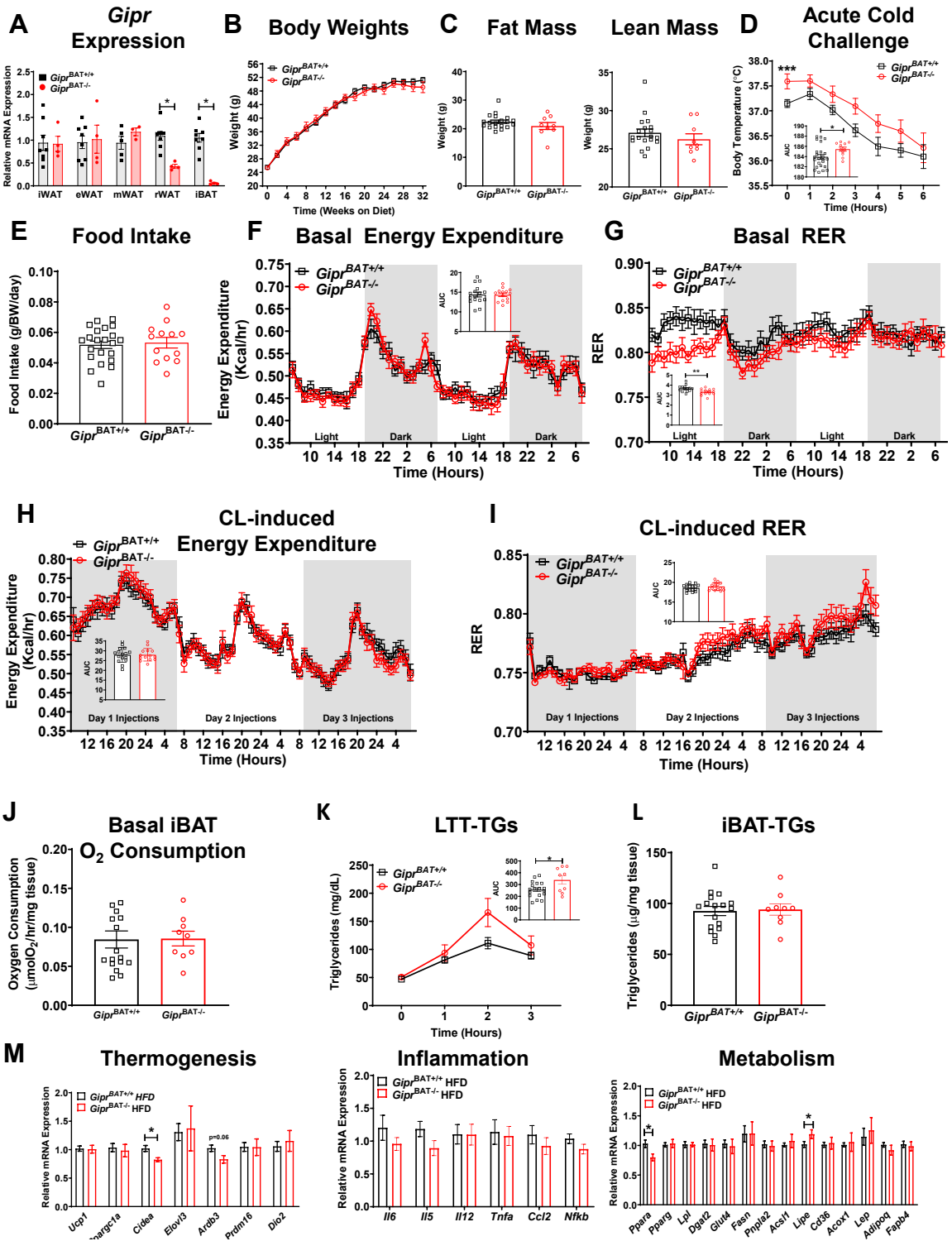

Figure 3: *Gipr*$^{BAT-/-}$ mice fed a HFD have normal body weight and food intake but lower basal RER and impaired lipid tolerance. (A) qPCR analysis of *Gipr* mRNA expression in adipose tissues from 4-week-old mice fed a RCD and housed at RT, n = 4–8. (B) Body weights in *Gipr*$^{BAT+/+}$ and *Gipr*$^{BAT-/-}$ mice (starting at 8–10 weeks of age), fed a HFD and housed at RT, n = 16–31. (C) Fat and lean mass, (D) temperature responses to acute cold challenge, AUC calculated from 0 to 5 hrs, and (E) food intake in *Gipr*$^{BAT+/+}$ and *Gipr*$^{BAT-/-}$ mice after 30 weeks, fed a HFD and housed at RT, n = 9–24. (F) Basal energy expenditure and (G) basal RER metabolic measurements in *Gipr*$^{BAT+/+}$ and *Gipr*$^{BAT-/-}$ mice after 16–18 weeks fed a HFD and housed at RT, n = 14–16. (H) energy expenditure and (I) RER in mice injected twice daily with CL316,243 after 16–18 weeks on HFD and housed at RT, n = 14–16. (J) *Ex vivo* basal O_2 consumption in iBAT from *Gipr*$^{BAT+/+}$ and *Gipr*$^{BAT-/-}$ mice, fed a HFD and housed at RT for 32 weeks, n = 9–17. (K) Levels of plasma triglycerides (TGs) during an oral lipid tolerance test (LTT), and (L) triglyceride content in iBAT from *Gipr*$^{BAT+/+}$ and *Gipr*$^{BAT-/-}$ mice, fed a HFD and housed at RT for 8–10 weeks, n = 9–18. (M) mRNA transcript levels in iBAT from *Gipr*$^{BAT+/+}$ and *Gipr*$^{BAT-/-}$ mice, fed a HFD housed at RT for 32 weeks, n = 6–16. *Tbp* was used to normalize relative mRNA expression levels. iBAT = interscapular brown adipose tissue. Data are represented as mean ± SEM. *p < 0.05, **p < 0.01, ***p < 0.001. See also Figure S2.

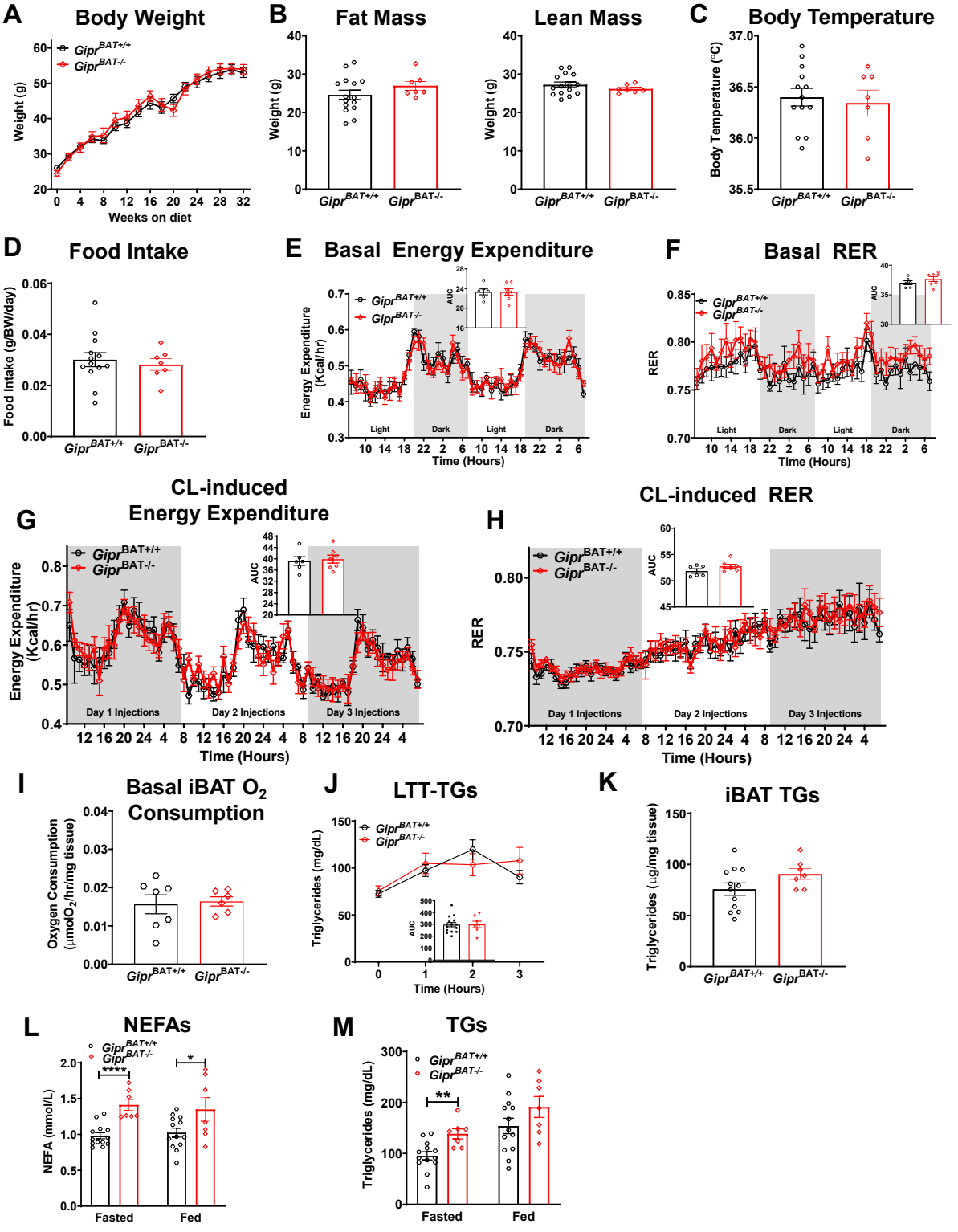

Figure 4: *Gipr*$^{BAT-/-}$ mice fed a HFD and housed at 30 °C have normal body weight, body temperatures, food intake and basal and CL-induced energy expenditure. (A) Body weights in *Gipr*$^{BAT+/+}$ and *Gipr*$^{BAT-/-}$ mice (starting at 8–10 weeks of age), (B) fat and lean mass, (C) body temperatures in fasted mice, and (D) food intake in *Gipr*$^{BAT+/+}$ and *Gipr*$^{BAT-/-}$ mice after 30–32 weeks fed a HFD and housed at 30 °C n = 7–13. (E) Basal energy expenditure and (F) basal RER metabolic measurements in *Gipr*$^{BAT+/+}$ and *Gipr*$^{BAT-/-}$ mice after 16–18 weeks fed a HFD and housed at 30 °C, n = 6–7. (G) Energy expenditure and (H) RER during twice-daily injections of CL316,243 for 3 days in *Gipr*$^{BAT+/+}$ and *Gipr*$^{BAT-/-}$ mice after 16–18 weeks fed a HFD and housing at 30 °C, n = 6–7. (I) *Ex vivo* basal O_2 consumption in iBAT from *Gipr*$^{BAT+/+}$ and *Gipr*$^{BAT-/-}$ mice, fed a HFD and housed at 30 °C for 32 weeks, n = 6–7. (J) Levels of plasma triglycerides (TGs) during an oral lipid tolerance test (LTT) and (K) triglyceride content in iBAT from *Gipr*$^{BAT+/+}$ and *Gipr*$^{BAT-/-}$ mice, fed a HFD and housed at 30 °C for 28 weeks, n = 7–15. (L) Plasma non-esterified fatty acids (NEFAs) after overnight fast and 1 hr refeed, and (M) plasma TGs in *Gipr*$^{BAT+/+}$ and *Gipr*$^{BAT-/-}$ mice, fed a HFD and housed at 30 °C for 28 weeks, n = 7–15. iBAT = interscapular brown adipose tissue. Data are represented as mean ± SEM. *p < 0.05, **p < 0.01, and ****p < 0.0001 See also Figure S3.

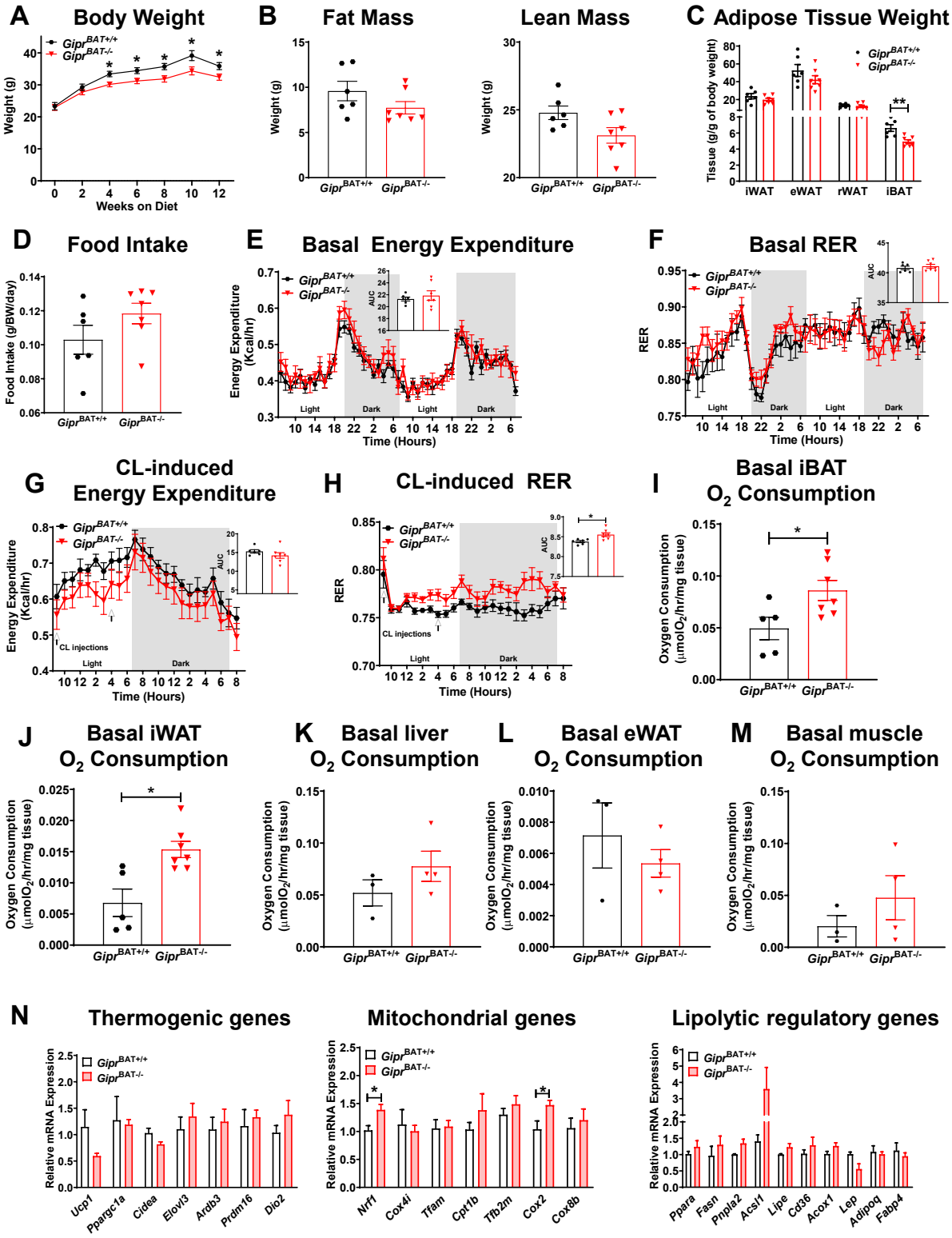

Figure 5: *Gipr*$^{BAT-/-}$ mice fed a HFD and housed at 4 °C have reduced body and iBAT weights, higher CL-induced RER and lipid tolerance. (A) Body weights in *Gipr*$^{BAT+/+}$ and *Gipr*$^{BAT-/-}$ mice (starting at 8–10 weeks of age), fed a HFD and housed at 4 °C, n = 6–7. (B) Fat and lean mass, (C) adipose tissue weights, and (D) food intake in *Gipr*$^{BAT+/+}$ and *Gipr*$^{BAT-/-}$ mice after 10–12 weeks on HFD and housed at 4 °C, n = 6–7. (E) Basal energy expenditure and (F) basal RER metabolic measurements in *Gipr*$^{BAT+/+}$ and *Gipr*$^{BAT-/-}$ mice after 10 weeks fed a HFD and housed at 4 °C, n = 6–7. (G) 24 hr Energy expenditure and (H) RER in response to two injections of CL316,243 in *Gipr*$^{BAT+/+}$ and *Gipr*$^{BAT-/-}$ mice after 10 weeks fed a HFD and housed at 4 °C, n = 6–7. *Ex vivo* basal O_2 consumption in iBAT (I), iWAT (J), liver (K), eWAT (L), and muscle (M) tissues from *Gipr*$^{BAT+/+}$ and *Gipr*$^{BAT-/-}$ mice, fed a HFD and housed at 4 °C for 6 weeks, n = 5–7. (N) mRNA transcript levels in iBAT from *Gipr*$^{BAT+/+}$ and *Gipr*$^{BAT-/-}$ mice, fed a HFD and housed at 4 °C for 12 weeks, n = 5–6. Levels of *Tbp* mRNA transcripts were used to normalize relative mRNA expression. iBAT = interscapular brown adipose tissue. Data are represented as mean ± SEM. *p < 0.05, **p < 0.01. See also Figure S4.

agonists in mice [25], short-term infusions of GIP in overweight or obese human subjects failed to inhibit food intake or modify energy expenditure [26]. Collectively, these findings highlight gaps in understanding how modulation of GIPR signaling impacts energy homeostasis.

In contrast to studies revealing a reduction of food intake and weight loss with selective GIPR agonists or co-agonists [21,27,28], attenuation of GIPR action also leads to prevention of weight gain in animal models of experimental obesity [8–11]. The majority of studies demonstrating that loss of GIPR signaling promotes resistance to weight gain were carried out in mice subjected to prolonged periods of HFD feeding [8,19,29–31]. The GIPR is highly expressed in WAT, and transgenic rescue of GIPR in WAT of *Gipr*$^{-/-}$ mice restored HFD-induced weight gain, albeit with an unexplained increase in lean and not adipose tissue mass [19]. Conversely, although reduction of GIPR signaling in WAT improved insulin sensitivity and decreased hepatosteatosis, loss of the WAT GIPR had no impact on the extent of weight gain after prolonged HFD feeding [32]. On the other hand, we observed resistance to obesity, improved glucose metabolism, and increased energy expenditure, in association with increased *Ucp1* expression in BAT in *Gipr*$^{-/-}$ mice fed a HFD [15]. Accordingly, we hypothesized that the BAT GIPR may contribute to one or more metabolic phenotypes evident in HFD-fed mice with global loss of GIPR signaling.

The data presented herein reveal that the GIPR is expressed and functional in BAT cells *in vitro*, and in murine BAT *in vivo*. Notably, gain and loss of GIPR signaling in BAT cells regulates genes important for inflammation and thermogenesis, and knockdown of the BAT *Gipr* increases levels of genes regulating thermogenesis, mitochondrial function, and lipid metabolism after CL316,243 treatment. Moreover, loss of the iBAT *Gipr* alters plasma NEFAs and TGs in *Gipr*$^{BAT-/-}$ mice studied at thermoneutrality. Even more striking are the phenotypes detected at 4 °C, including resistance to weight gain, reduced BAT weight, a shift in RER after CL316,243, and increased oxygen consumption in WAT and BAT. Hence, under conditions favoring BAT activation, loss of the BAT GIPR shifts the metabolic profile of BAT to favor energy expenditure.

Interestingly, GIP regulates IL-6 gene expression and secretion in BAT cells, whereas knockdown of *Gipr* markedly decreased *Il6* mRNA transcripts. Furthermore, GIP increased plasma IL-6 levels in mice. Concordant regulation of *IL6* and *GIPR* mRNA transcripts was reported in human WAT following exercise [33], and GIP directly induced *IL6* mRNA and IL-6 secretion in human adipocytes *ex vivo* [34] and IL6 mRNA was increased in human adipose tissue following 4 hrs of GIP infusion in the postprandial state [35]. Conversely, plasma IL-6 levels were reduced in HFD-fed *Gipr*$^{Adipo-/-}$ mice [32]. GIP also stimulated IL-6 production from murine and human α-cells *ex vivo*. Hence, our data linking BAT GIPR to control of IL-6 expression adds to growing evidence linking gain and loss of GIPR signaling to control of IL-6 levels, findings with possible relevance for understanding how GIP activity controls local and systemic inflammation.

Our current data demonstrating functional activity of the BAT GIPR adds to the growing body of literature linking the partial or complete absence of GIP activity with resistance to weight gain or weight loss. Experimental and clinical states of nutrient excess and obesity are associated with increased circulating levels of GIP, enhanced inflammation, and adipose tissue accretion [2,36]. Indeed, *Gipr*$^{-/-}$ mice resist weight gain in response to diets enriched in fat content, but not after exposure to a carbohydrate-enriched diet [37]. Conversely, mice heterozygous for inactivation of one allele of the *Gip* gene exhibit resistance to weight gain, higher fat oxidation and energy expenditure, and preservation of insulin sensitivity after HFD feeding [9]. Nevertheless, GIPR agonism also reduces food intake in mice [27], and transgenic overexpression of GIP promotes resistance to diet-induced obesity and reduced fat mass in mice [38]. Hence, the direct and indirect actions of GIP on adipose tissue and whole body energy homeostasis are complex and highly context-dependent.

Extending data from genetic manipulation of the *Gipr*, a series of monoclonal antibodies against the GIPR attenuated weight gain in mice and non-human primates, with modest reductions in food intake and a reduction in RER, consistent with greater lipid oxidation [11]. These findings were preserved in *Gipr*$^{\beta cell-/-}$ mice, dissociating attenuation of weight gain from the consequences of diminished GIPR signaling within islet β-cells. Moreover, the reported changes in RER are consistent with our findings in *Gipr*$^{BAT-/-}$ mice and identify the GIPR in BAT as a potential component of mechanisms governing the control of fuel oxidation and lipid metabolism. Nonetheless, our studies failed to detect compelling body weight phenotypes in *Gipr*$^{BAT-/-}$ mice studied at room temperature and thermoneutrality and we did not observe increased energy expenditure in *Gipr*$^{BAT-/-}$ mice. Hence, selective loss of the GIPR in BAT is insufficient to phenocopy metabolic findings arising in HFD-fed mice or monkeys studied at room temperature with systemic reduction of GIP activity [11].

The findings that GIP immunoneutralization [39] or blockade of the GIPR with antibodies [11] reproduces the resistance to diet-induced obesity phenotype localizes some of the metabolic actions of the GIPR to peripheral tissues, as these antibodies are unlikely to block GIPR signaling in the central nervous system. Recent studies have identified a role for the myeloid GIPR in the suppression of the alarmin S100A/9 within a subset of macrophages. Notably, the reduction of immune cell GIPR expression led to more significant weight gain and impaired energy expenditure in HFD-fed mice [40]. Alternatively, central regulation of GIPR signaling modifies hypothalamic leptin sensitivity, consistent with the failure of reduced GIP action to attenuate the hyperphagia of *ob*/*ob* mice [41]. Hence, multiple mechanisms and cell types contribute to how GIPR signaling controls energy homeostasis.

Together, our present findings define multiple functional roles for the GIPR in BAT associated with changes in gene expression, IL-6 expression and secretion, oxygen consumption *ex vivo*, lipid utilization, the defence of body temperature, and metabolism. However, loss of the BAT GIPR alone is insufficient to recapitulate the resistance to diet-induced obesity or weight loss described in HFD-fed mice or monkeys with loss of GIP action [8,9].

4.1. Limitations

We acknowledge that our studies have several limitations. First, we only performed experiments in male mice. Previously published data assessing body weight phenotypes were carried out predominantly in male whole body *Gipr*$^{-/-}$ mice; therefore, for comparative purposes, we limited our studies to males. We studied mice without experimental diabetes; hence, whether dysglycemic states modify the metabolic activity of GIPR-deficient BAT is not known. Furthermore, although we observed lower body weight in *Gipr*$^{BAT-/-}$ mice housed at 4 °C, we did not identify any differences in energy expenditure, possibly because mice were switched from housing at 4°C for subsequent analysis of energy expenditure under normal room temperature conditions. Finally, we did not carry out chronic studies with selective GIPR agonists; hence, the putative importance of the presence and absence of the BAT GIPR for the metabolic responses to sustained GIPR activation remains to be determined.

AUTHOR CONTRIBUTIONS

Conceptualization, J.L.B. H.E.B., J.E.C., and D.J.D.; Methodology, J.L.B., K.D.K., and J.E.C.; Investigation, J.L.B., K.D.K., E.M.V., L.L.B., X.C., E.E.M., H.E.B., and J.E.C.; Writing-Original Draft, J.L.B., K.D.K., and D.J.D.; Writing-Review & Editing, J.L.B., K.D.K., E.M.V., L.L.B., X.C., E.E.M., H.E.B., J.E.C., and D.J.D.; Supervision, J.E.C. and D.J.D.

ACKNOWLEDGEMENTS

J.L.B. and E.M.V. have received fellowship funding from Diabetes Canada. E.E.M. has received fellowship funding from the Canadian Diabetes Association and the Canadian Institutes of Health Research. H.E.B. has received fellowships from the Canadian Diabetes Association and the Banting and Best Diabetes Centre, University of Toronto. J.E.C. has received fellowships from the Banting and Best Diabetes Centre, University of Toronto, and the Canadian Institutes of Health Research. D.J.D. is supported by the Banting and Best Diabetes Centre-Novo Nordisk Chair in Incretin Biology, CIHR grant 154321 and investigator-initiated operating grant support from Novo Nordisk Inc.

CONFLICT OF INTEREST

D.J.D. has served as a speaker for Eli Lilly and as an advisor or consultant to Intarcia, Kallyope, Merck Research Laboratories, Pfizer, Novo Nordisk and Sanofi. Mt. Sinai receives investigator-initiated funding from Merck, Novo Nordisk, and Shire, a division of Takeda Inc, for preclinical studies of peptide biology in the Drucker laboratory. E.E.M. has received speaker's honoraria from Merck Canada, and the Ottawa Heart Institute receives funding from Merck for preclinical studies in the Mulvihill laboratory. J.E.C. has received speaker honoraria from Merck, and Duke Molecular Physiology Institute receives funding from Eli Lilly for preclinical studies in the Campbell laboratory. The other authors have no other conflicts of interest relevant to this article to disclose.

APPENDIX A. SUPPLEMENTARY DATA

Supplementary data to this article can be found online at https://doi.org/10.1016/j.molmet.2019.08.006.

REFERENCES

[1] Drucker, D.J., 2007. The role of gut hormones in glucose homeostasis. Journal of Clinical Investigation 117(1):24–32.

[2] Campbell, J.E., Drucker, D.J., 2013. Pharmacology physiology and mechanisms of incretin hormone action. Cell Metabolism 17(4):819–837.

[3] Drucker, D.J., Habener, J.F., Holst, J.J., 2017. Discovery, characterization, and clinical development of the glucagon-like peptides. Journal of Clinical Investigation 127(12):4217–4227.

[4] Finan, B., Muller, T.D., Clemmensen, C., Perez-Tilve, D., DiMarchi, R.D., Tschop, M.H., 2016. Reappraisal of GIP pharmacology for metabolic diseases. Trends in Molecular Medicine 22(5):359–376.

[5] Deacon, C.F., 2004. Therapeutic strategies based on glucagon-like peptide 1. Diabetes 53(9):2181–2189.

[6] Mulvihill, E.E., Drucker, D.J., 2014. Pharmacology, physiology and mechanisms of action of dipeptidyl peptidase-4 inhibitors. Endocrine Reviews, 6992-1019.

[7] Hojberg, P.V., Vilsboll, T., Rabol, R., Knop, F.K., Bache, M., Krarup, T., et al., 2009. Four weeks of near-normalisation of blood glucose improves the insulin response to glucagon-like peptide-1 and glucose-dependent insulinotropic polypeptide in patients with type 2 diabetes. Diabetologia 52(2):199–207.

[8] Miyawaki, K., Yamada, Y., Ban, N., Ihara, Y., Tsukiyama, K., Zhou, H., et al., 2002. Inhibition of gastric inhibitory polypeptide signaling prevents obesity. Nature Medicine 8(7):738–742.

[9] Nasteska, D., Harada, N., Suzuki, K., Yamane, S., Hamasaki, A., Joo, E., et al., 2014. Chronic reduction of GIP secretion alleviates obesity and insulin resistance under high-fat diet conditions. Diabetes 63(7):2332–2343.

[10] Boylan, M.O., Glazebrook, P.A., Tatalovic, M., Wolfe, M.M., 2015. Gastric inhibitory polypeptide immunoneutralization attenuates development of obesity in mice. American Journal of Physiology Endocrinology and Metabolism 309(12):E1008–E1018.

[11] Killion, E.A., Wang, J., Yie, J., Shi, S.D., Bates, D., Min, X., et al., 2018. Anti-obesity effects of GIPR antagonists alone and in combination with GLP-1R agonists in preclinical models. Science Translational Medicine 10(472).

[12] Speliotes, E.K., Willer, C.J., Berndt, S.I., Monda, K.L., Thorleifsson, G., Jackson, A.U., et al., 2010. Association analyses of 249,796 individuals reveal 18 new loci associated with body mass index. Nature Genetics 42(11):937–948.

[13] Wen, W., Cho, Y.S., Zheng, W., Dorajoo, R., Kato, N., Qi, L., et al., 2012. Meta-analysis identifies common variants associated with body mass index in east Asians. Nature Genetics 44(3):307–311.

[14] Nakayama, K., Watanabe, K., Boonvisut, S., Makishima, S., Miyashita, H., Iwamoto, S., 2014. Common variants of GIP are associated with visceral fat accumulation in Japanese adults. American Journal of Physiology Gastrointestinal and Liver Physiology 307(11):G1108–G1114.

[15] Hansotia, T., Maida, A., Flock, G., Yamada, Y., Tsukiyama, K., Seino, Y., et al., 2007. Extrapancreatic incretin receptors modulate glucose homeostasis, body weight, and energy expenditure. Journal of Clinical Investigation 117(1):143–152.

[16] Miyawaki, K., Yamada, Y., Yano, H., Niwa, H., Ban, N., Ihara, Y., et al., 1999. Glucose intolerance caused by a defect in the entero-insular axis: a study in gastric inhibitory polypeptide receptor knockout mice. Proceedings of the National Academy of Sciences of the United States of America 96(26):14843–14847.

[17] Campbell, J.E., Ussher, J.R., Mulvihill, E.E., Kolic, J., Baggio, L.L., Cao, X., et al., 2016. TCF1 links GIPR signaling to the control of beta cell function and survival. Nature Medicine, 2284–2290.

[18] Uldry, M., Yang, W., St-Pierre, J., Lin, J., Seale, P., Spiegelman, B.M., 2006. Complementary action of the PGC-1 coactivators in mitochondrial biogenesis and brown fat differentiation. Cell Metabolism 3(5):333–341.

[19] Ugleholdt, R., Pedersen, J., Bassi, M.R., Fuchtbauer, E.M., Jorgensen, S.M., Kissow, H.L., et al., 2011. Transgenic rescue of adipocyte glucose-dependent insulinotropic polypeptide receptor expression restores high fat diet-induced body weight gain. Journal of Biological Chemistry 286(52):44632–44645.

[20] Sanchez-Gurmaches, J., Hung, C.M., Sparks, C.A., Tang, Y., Li, H., Guertin, D.A., 2012. PTEN loss in the Myf5 lineage redistributes body fat and reveals subsets of white adipocytes that arise from Myf5 precursors. Cell Metabolism 16(3):348–362.

[21] Finan, B., Ma, T., Ottaway, N., Muller, T.D., Habegger, K.M., Heppner, K.M., et al., 2013. Unimolecular dual incretins maximize metabolic benefits in rodents, monkeys, and humans. Science Translational Medicine 5(209), 209ra151.

[22] Frias, J.P., Bastyr 3rd, E.J., Vignati, L., Tschop, M.H., Schmitt, C., Owen, K., et al., 2017. The sustained effects of a dual GIP/GLP-1 receptor agonist, NNC0090-2746, in patients with type 2 diabetes. Cell Metabolism 26(2):343–352 e342.

[23] Coskun, T., Sloop, K.W., Loghin, C., Alsina-Fernandez, J., Urva, S., Bokvist, K.B., et al., 2018. LY3298176, a novel dual GIP and GLP-1 receptor agonist for the treatment of type 2 diabetes mellitus: from discovery to clinical proof of concept. Molecular Metabolism 18:3–14.

[24] Frias, J.P., Nauck, M.A., Van, J., Kutner, M.E., Cui, X., Benson, C., et al., 2018. Efficacy and safety of LY3298176, a novel dual GIP and GLP-1 receptor agonist, in patients with type 2 diabetes: a randomised, placebo-

controlled and active comparator-controlled phase 2 trial. Lancet 392(10160):2180–2193.

[25] Norregaard, P.K., Deryabina, M.A., Tofteng Shelton, P., Fog, J.U., Daugaard, J.R., Eriksson, P.O., et al., 2018. A novel GIP analogue, ZP4165, enhances glucagon-like peptide-1-induced body weight loss and improves glycaemic control in rodents. Diabetes Obesity and Metabolism 20(1):60–68.

[26] Bergmann, N.C., Lund, A., Gasbjerg, L.S., Meessen, E.C.E., Andersen, M.M., Bergmann, S., et al., 2019. Effects of combined GIP and GLP-1 infusion on energy intake, appetite and energy expenditure in overweight/obese individuals: a randomised, crossover study. Diabetologia 62(4):665–675.

[27] Mroz, P.A., Finan, B., Gelfanov, V., Yang, B., Tschop, M.H., DiMarchi, R.D., et al., 2019. Optimized GIP analogs promote body weight lowering in mice through GIPR agonism not antagonism. Molecular Metabolism 20: 51–62.

[28] Finan, B., Yang, B., Ottaway, N., Smiley, D.L., Ma, T., Clemmensen, C., et al., 2015. A rationally designed monomeric peptide triagonist corrects obesity and diabetes in rodents. Nature Medicine 21(1):27–36.

[29] Zhou, H., Yamada, Y., Tsukiyama, K., Miyawaki, K., Hosokawa, M., Nagashima, K., et al., 2005. Gastric inhibitory polypeptide modulates adiposity and fat oxidation under diminished insulin action. Biochemical and Biophysical Research Communications 335(3):937–942.

[30] McClean, P.L., Irwin, N., Cassidy, R.S., Holst, J.J., Gault, V.A., Flatt, P.R., 2007. GIP receptor antagonism reverses obesity, insulin resistance and associated metabolic disturbances induced in mice by prolonged consumption of high fat diet. American Journal of Physiology Endocrinology and Metabolism 293(6): E1746–E1755.

[31] Bates, H.E., Campbell, J.E., Ussher, J.R., Baggio, L.L., Maida, A., Seino, Y., et al., 2012. Gipr is essential for adrenocortical steroidogenesis; however, corticosterone deficiency does not mediate the favorable metabolic phenotype of Gipr(-/-) mice. Diabetes 61(1):40–48.

[32] Joo, E., Harada, N., Yamane, S., Fukushima, T., Taura, D., Iwasaki, K., et al., 2017. Inhibition of gastric inhibitory polypeptide receptor signaling in adipose tissue reduces insulin resistance and hepatic steatosis in high-fat diet-fed mice. Diabetes 66(4):868–879.

[33] Dekker, M.J., Graham, T.E., Ooi, T.C., Robinson, L.E., 2010. Exercise prior to fat ingestion lowers fasting and postprandial VLDL and decreases adipose tissue IL-6 and GIP receptor mRNA in hypertriacylglycerolemic men. The Journal of Nutritional Biochemistry 21(10):983–990.

[34] Timper, K., Grisouard, J., Sauter, N.S., Herzog-Radimerski, T., Dembinski, K., Peterli, R., et al., 2013. Glucose-dependent insulinotropic polypeptide induces cytokine expression, lipolysis, and insulin resistance in human adipocytes. American Journal of Physiology Endocrinology and Metabolism 304(1):E1–E13.

[35] Gogebakan, O., Osterhoff, M.A., Schuler, R., Pivovarova, O., Kruse, M., Seltmann, A.C., et al., 2015. GIP increases adipose tissue expression and blood levels of MCP-1 in humans and links high energy diets to inflammation: a randomised trial. Diabetologia 58(8):1759–1768.

[36] Goralska, J., Razny, U., Polus, A., Stancel-Mozwillo, J., Chojnacka, M., Gruca, A., et al., 2018. Pro-inflammatory gene expression profile in obese adults with high plasma GIP levels. International Journal of Obesity (London) 42(4):826–834.

[37] Maekawa, R., Ogata, H., Murase, M., Harada, N., Suzuki, K., Joo, E., et al., 2018. Glucose-dependent insulinotropic polypeptide is required for moderate high-fat diet- but not high-carbohydrate diet-induced weight gain. American Journal of Physiology Endocrinology and Metabolism 314(6):E572–E583.

[38] Kim, S.J., Nian, C., Karunakaran, S., Clee, S.M., Isales, C.M., McIntosh, C.H., 2012. GIP-overexpressing mice demonstrate reduced diet-induced obesity and steatosis, and improved glucose homeostasis. PLoS One 7(7):e40156.

[39] Fulurija, A., Lutz, T.A., Sladko, K., Osto, M., Wielinga, P.Y., Bachmann, M.F., et al., 2008. Vaccination against GIP for the treatment of obesity. PLoS One 3(9):e3163.

[40] Mantelmacher, F.D., Zvibel, I., Cohen, K., Epshtein, A., Pasmanik-Chor, M., Vogl, T., et al., 2019. An enteroendocrine-myeloid cell S100A8/A9 axis controls inflammation and body weight. Nature Metabolism 158:69.

[41] Shimazu-Kuwahara, S., Harada, N., Yamane, S., Joo, E., Sankoda, A., Kieffer, T.J., et al., 2017. Attenuated secretion of glucose-dependent insulinotropic polypeptide (GIP) does not alleviate hyperphagic obesity and insulin resistance in ob/ob mice. Molecular Metabolism 6(3):288–294.

